Heat Transfer Performance of Falling Film Type Plate-fin Evaporator

Journal of National Fisheries University 64 (4) 283 − 291 (2016)

Heat Transeer Performance of Falling Film Type Plate-Fin Evaporator

Junichi Ohara

Abstract：The characteristics of heat transfer and flow patterns are investigated experimentally for the vertical falling film evaporation of pure refrigerant HCFC123 in a rectangular minichannels consisting of offset strip fins. The refrigerant liquid is uniformly supplied to the channel through a distributor. The liquid flowing down vertically is heated electrically from the rear wall of the channel and evaporated. To observe the flow patterns during the evaporation process directly, a transparent vinyl chloride resin plate is placed as the front wall. The experimental parameters are as follows: the mass velocity $G =$ 28~70 kg/(m^{2}s), the heat flux $q =$ 20~50 kW/m^2 and the pressure $P \approx$ 100 kPa. It is clarified that the heat transfer coefficient a depends on G and q in the region of vapor quality $x \geq$ 0.3 while there is little influence of G and q in the region $x \leq 0.3$. From the direct observation using a high speed video camera and a digital still camera, flow patterns are classified into five types. Then the empirical correlation equations for evaporation heat transfer coefficient on a vertical falling film plate fin evaporator with minichannels are proposed. From the physical model to evaluate the heat transfer coefficient of the minichannel surface with fins, the characteristics of fin efficiency is clarified that the average value of fin efficiency is about 0.6 and the distributive characteristics of fin efficiency is roughly inverse of heat transfer coefficient characteristics.

Key words：Minichannels, Heat transfer, Plate Fin Evaporator, Falling film

Introduction

Recently, nonazeotropic refrigerant mixtures (NARMs), which are composed of environmentally acceptable alternatives, have become of special interest in the use as working fluid in vapor compression heat pump/refrigeration cycles. Previous studies on evaporation and condensation of NARMs, however, reported that the heat transfer coefficients of NARMs are lower than those of pure refrigerant. To compensate for this defect, it is necessary to improve the performance of heat exchangers. From this point of view, special interests have been taken in plate fin heat exchangers. Focusing on evaporators, falling liquid type plate fin evaporators that have standout features of high heat transfer rate at small temperature difference even in the case of small mass velocity of refrigerants are considered as one of the promising evaporators to improve the performance of heat pump/refrigeration cycles using NARMs as working fluids.

Robertson and Lovegrove[1] conducted flow boiling experiments with CFC 11 vertically up through the electrically heated offset strip fin test section. Thome[2] introduced plate fin heat exchanger as an important alternative to enhanced boiling tubes for augmenting boiling heat transfer and summarized previous studies on boiling in plate fin heat exchanger. Kandlikar[3] proposed the additive model of the convective and nucleate boiling components for flow boiling heat transfer in offset strip fin evaporator using the data obtained by Rovertson and Loveglove [1]. Feldman et al.[4] obtained local heat transfer characteristics of CFC114 experimentally in a plate fin evaporator with offset strip and perforated fin surface and proposed a correlation equation taking into account the

Department of Ocean Mechanical Engineering, National Fisheries University,
Shimonoseki, Yamaguchi, Japan

dominance of nucleate boiling and convective boiling. Watel [5] had compiled the review for heat transfer characteristics of flow boiling in compact heat exchangers that have small passages of straight, perforated and offset strip fin. The typical trends of local heat transfer coefficient show that it is easy to distinguish between the two dominant mechanisms of boiling. Kim and Sohn[6] reported that an experimental study on saturated flow boiling heat transfer of R113 in a vertical rectangular channel with offset strip fins. The predictions of local flow boiling heat transfer coefficients were found to be in good agreement with experimental data. An experimental study on saturated flow boiling heat transfer of HFE-7100 in vertical rectangular channels with offset strip fins is presented by Pulvirenti et al.[7]. The local boiling heat transfer coefficient has been obtained from experiments and analyzed by means of Chen superposition method. Some correlations for convective and nucleate boiling heat transfer coefficients have been found that agree well with the obtained data.

Most of them reviewed above have been carried out on the condition that test fluid flows up vertically, but few studies on the downflow condition. At the same time, a number of studies are conducted and reported about flow boiling heat transfer characteristics of falling liquid film that flows down on the plane walls, the inside and the outside wall of the tubes and horizontal tube banks other than offset strip fin surface in plate fin heat exchanger.

Ribatski and Jacobi[8] reviewed studies for falling film evaporation on horizontal tubes. It covers flow-pattern studies, and the experimental parameters that affect the heat transfer performance on plain single tubes, enhanced surfaces and tube bundles. An experimental study of falling film heat transfer outside horizontal tubes was carried out by Yang and Shen[9] in order to show how the heat transfer coefficient is affected by different parameters such as evaporation temperatures, temperature difference between wall and saturation water and so on. The results show that the heat transfer coefficient increases with the increase in liquid feeding, evaporation boiling temperature and heat flux. An experimental study of heat and mass transfer in free and forced convection in a vertical channel with parallel metal plates is presented by Cherif et al.[10]. The results obtained are exploited to study the influence of the operating parameters such as the heat flux.

As shown above, there are very few literatures about falling film evaporation in a plate fin heat exchanger. In the present study, to clarify the heat transfer and flow pattern characteristics in a plate fin evaporator on the downflow condition, the vertical falling film evaporation of pure refrigerant HCFC123 in a rectangular minichannel consisting of offset strip fins was investigated experimentally.

NOMENCLATURE

A	: area of heat transfer	[m_2]
C_p	: isobaric specific heat	[J/(kg K)]
d_h	: hydraulic diameter	[m]
G	: refrigerant mass velocity	[kg/(m_2s)]
h	: specific enthalpy	[kJ/kg]
Nu	: Nusselt number $= adh/\lambda_l$	[-]
P	: pressure	[Pa]
Pr_1	: Prandtl Number $= \mu_l C_{pl}/\lambda_l$	[-]
Q	: heat transfer rate	[W]
q	: heat flux	[W/m_2]
Re_1	: liquid Reynolds number $= G(1-x)d_h/\mu_l$	[-]
Re_{lv}	: vapor Reynolds number $= Gxd_h/\mu_v$	[-]
	: two phase Reynolds number $= Gxd_h/\rho_v v_l$	[-]
S	: cross sectional area	[m_2]
T	: temperature	[K]
W	: mass flow rate	[kg/s]
x	: vapor quality	[-]
a	: heat transfer coefficient	[W/(m_2K)]
λ	: thermal conductivity	[W/(m K)]
μ	: dynamic viscosity	[Pas]
ρ	: density	[kg/m^3]
X_u	: Lockhart-Martinelli parameter $=(1-x/x)^{0.9}(\rho_v/\rho_l)^{0.5}(\mu_l/\mu_v)^{0.1}$	[-]

Subscript

B	: base	lo	: liquid only
b	: bulk	r	: refrigerant
f	: fin	sat	: saturation state
i	: section number	v	: vapor
l	: liquid	w	: wall

EXPERIMANTAL APPARATUS AND MEASUREMENT METHOD

Experimental Apparatus

Figure 1 shows schematic view of the present experimental apparatus. The refrigerant loop is a forced circulation one which

consists of main and by-pass loops. The refrigerant liquid discharged by a gear pump (1) branches into the main and the by-pass loops. A valve in the by-pass loop (14) is used to control the refrigerant flow rate in the main loop. In the main loop, the liquid flows into a preheater (3) through a mass flow meter (2) and a mixing chamber; in the preheater the liquid is heated close to saturation state. Then, the liquid is introduced into a test evaporator (6) by a distributor (5) through a mixing chamber and a dividing chamber (4). In the evaporator the liquid flowing down vertically is heated electrically and evaporated. The vapor generated in the evaporator is condensed to the liquid by a plate-fin condenser (7). This liquid together with unevaporated liquid in the evaporator is returned to the pump (1) through a subcooler (9) which is used to prevent the liquid from evaporating in the pump.

Figure 2 shows the schematic view of the test evaporator, which is a vertical rectangular channel with an offset strip fin surface. The fins and base plate are made of aluminum alloy and both of them are vacuum-brazed each other. The cross-sectional area of the channel is 6.35mm × 190mm, and the effective heating length is 1000mm. A 30 mm thick transparent vinyl chloride resin plate is placed as the front wall of the channel in order to observe the flow pattern during the evaporation process directory. The rear wall is divided into 10 sections of same dimensions, each of which is heated by a 100 mm long sheet type electric heater. The electric input of these heaters can be controlled individually. A rectangular liquid distributor is set at the top of the channel to supply refrigerant liquid uniformly. The electric input of these heaters can be controlled individually. A rectangular liquid distributor is set at the top of the channel to supply refrigerant liquid uniformly. In the distributor, the liquid is introduced into the rectangular part from both ends, and spouted out from 37 holes of 0.9 mm I.D. on the surface facing downward. Prior to the experiment on heat transfer, the performance of the liquid distributor is examined. It is found that the distribution characteristics are independent of mass flow rate of working fluid and refrigerant liquid can be distributed uniformly within 5% deviation over the whole width of the test evaporator. Details of performance on liquid distribution were described by Ohara and Koyama [11]. For a reference, Figure 3 shows the configuration of fin in detail, and Table 1 shows the specification for the test evaporator.

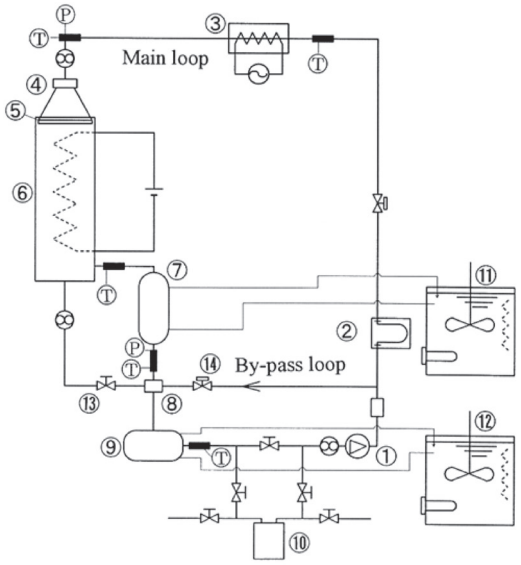

Fig. 1. Schematic of experimental apparatus

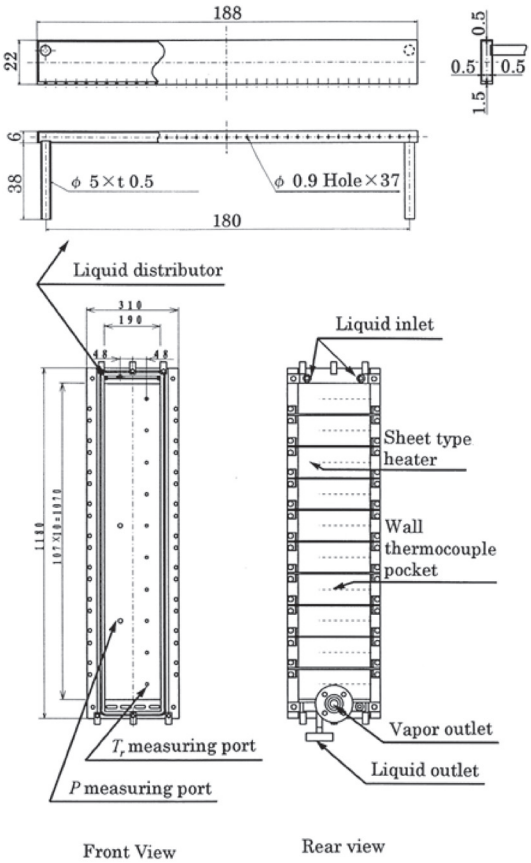

Fig. 2. Schematic view of the test evaporator

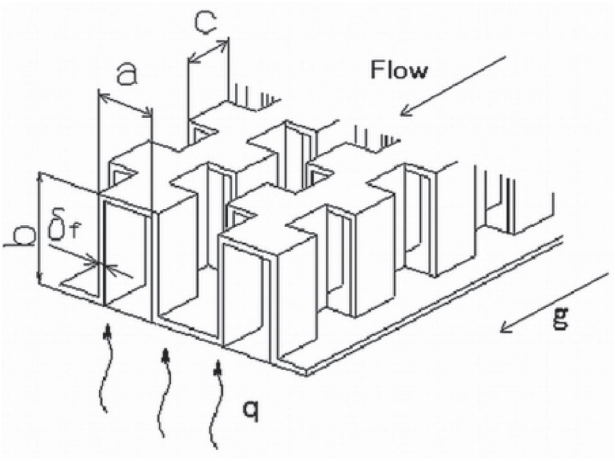

Fig. 3. Schematic view of the test evaporator

Table 1. Specification of test evaporator

Fin Type		Offset strip
Fin Spacing	a [mm]	1.478
Fin Height	b [mm]	6.35
Fin Thickness	δ_f [mm]	0.203
Hydraulic Diameter	d_h [mm]	2.11
Width of refrigerant channel	. [mm]	190
Effective Heat Transfer Length	. [mm]	1000
Number of Section		10
Cross-sectional Area	[m^2]	1.02×10^{-3}
Base Surface Area	[m^2]	0.202
Real Surface Area	[m^2]	2.056
Increased Ratio of Surface Area		10.18

Measurement Method

The heat loss is evaluated ignorable for the following reasons. [1] In the case of refrigerant mass velocity G = 28 kg/(m^2s) and heat flux q = 50 kW/m^2, rear surface temperature reaches its maximum about 170 degree Celsius, and total of estimated free convective heat transfer rate and heat transfer rate by radiation from rear surface without insulation is 891W/m^2. The heat loss becomes only 1.8% of total. [2] The rear surface of the test evaporator was covered by 80mm thick rockwool for heat insulation. [3] The temperature of the room where experiments was carried out was kept about 28 degrees C near the saturation temperature of test refrigerant. Because of the negligible heat loss from the evaporator to the ambient, the heat transfer rate to the refrigerant in each section is supposed to be equal to the electric power of a heater, which is evaluated from the voltage drop through it and the electric current flowing through a standard resistance connected in series. Refrigerant mass flow rate is measured by a micro-motion mass flow meter. The refrigerant temperature is measured at each section of the test evaporator with a φ 1.6 mm K-type thermocouple inserted in the refrigerant channel through the transparent plate. The wall temperature at the center of each section is measured with a φ 0.5 mm K-type thermocouple inserted through a capillary tube (0.9 mm I.D.) laid in the wall. This thermocouple is traveled in the capillary tube in order to evaluate the average wall temperature. The refrigerant pressure is measured at upper part of the test evaporator, centers of 5th and 8th sections and outlet of evaporator with absolute pressure transducers set at the ports on the transparent plate. The calibration errors of sensors are summarized in Table 2. And the evaluation of the accuracy in the determination of the local heat transfer coefficient gives average relative error of 14% by use of each experimental data. From definition of heat transfer coefficient, the relative error consists of heat flux term and term of temperature difference between the wall and the saturated fluid, and the term of temperature difference relatively increased when the temperature difference becomes smaller (about 2K) in the high heat transfer region.

Table 2: The calibration errors of sensors

Measurement	Type of Sensor	Accuracy
Refrigerant Temperature (Test Section)	K-Type Thermocouple	± 0.01 degrees C
Wall Temperature (Test Section)	K-Type Thermocouple	±0.01 degrees C
Pressure	Pressure Transducer	±0.01 kPa
Refrigerant flow Rate	Micro-motion Mass Flow Meter	±0.3 R.D.
Power Input	Standard Resistance	±0.01 mΩ

The experiments are carried out with the following range: the refrigerant saturation pressure $P_{sat} \approx$ 100kPa, uniform heat flux from 2nd to 10th sections q = 20, 30, 40 and 50 kW/m^2, and to clarify the heat transfer characteristics in small range of mass velocity, the value of refrigerant mass velocities are chosen as G = 28, 40, 55 and 70 kg/(m^2s).

DATA REDUCTION

The specific enthalpy of subcool liquid flowing into the evaporator is evaluated from the refrigerant pressure and temperature, both of which are measured at the mixing chamber set just before the evaporator.

$$h_{b0} = h_l(P, T_r) \quad (1)$$

The bulk enthalpy at the outlet of the i th section h_{bi} is

calculated as

$$h_{bi} = h_{b(i-1)} + \frac{Q_i}{W} \quad (i=1,2\ldots,10) \tag{2}$$

where Q_i is the heat transfer rate of the i th section, and W is the refrigerant mass flow rate. Then the quality at the outlet of the i th section x_i is calculated as

$$x_i = \frac{h_{bi} - h_{lsat}}{h_{vsat} - h_{lsat}} \tag{3}$$

where h_{vsat} and h_{lsat} denote the enthalpy of vapor and liquid at saturation state, which is evaluated by the measured pressure. The quality at the center of the i th section is calculated as arithmetic average one between inlet and outlet of the i th section. The local heat transfer coefficient is defined as

$$a_i \equiv \frac{Q_i}{A_B(T_{wi} - T_{sati})} = \frac{q_i}{T_{wi} - T_{sati}} \tag{4}$$

where A_B , q and T_{wi} are the base heat transfer area, the local heat flux and the wall temperature of the i th section, respectively, and T_{sai} is the saturation temperature at the center of the i th section, which is estimated from the pressure distribution. The mass velocity G is defined as

$$G = \frac{W}{S} \tag{5}$$

where, S is the cross-sectional area excluding the sum of fin cross-sectional area. The thermodynamic and transport property of HCFC123 are estimated by use of REFPROP ver.7.

RESULTS AND DISCUSSIONS

Distribution of Temperature, Pressure and Quality

Figure 4 shows an example of the distribution of temperature, pressure and quality in the refrigerant flow direction on the condition of heat flux q = 50 kW/m^2 and refrigerant mass velocity G= 55 kg/(m^{2}s). Symbols of solid circle, solid triangle, solid inverted triangle and triangle denote refrigerant temperature T_r, wall temperature T_w, pressure P, and heat flux q, respectively; all data of T_r and T_w are measured values. The pressure measurement ports of the test evaporator are set at the inlet, the 5th section, the 8th section and the outlet, so pressure data of other sections are interpolated data. Symbols of solid square and circle denote saturation state temperature T_{sat} and quality x ; these are calculated values. Integer and MIX on the abscissa represent the section number and the mixing chamber just before the test evaporator. In this case, the 1st section is heated at 15 kW/m^{2}for preheating, and the others are heated uniformly at 50

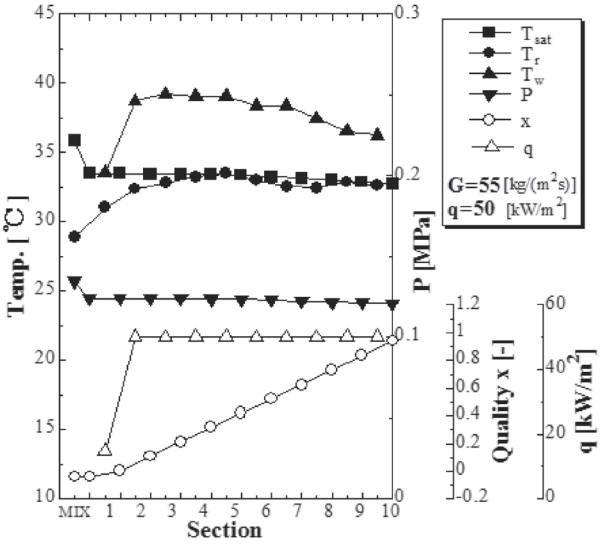

Fig. 4. Distribution of temperature, heat flux and quality

kW/m^2. The value of T_r increases gradually toward the downstream from the inlet, and approaches T_{sat} after the 3rd section. The value of T_w increases sharply between the 1st and the 2nd sections, and remains constant from the 2nd to the 5th sections. After the 5th section, it decreases gradually in the flow direction. The value of x increases linearly in the flow direction because of the uniform heat flux from the 2nd to the 10th sections. Through all the experiments, the subcooling of the refrigerant liquid at the inlet of the test evaporator is ranged from 0.5 to 7.0 K. The average pressure drop between inlet and outlet of the test evaporator are 1.4 kPa. Saturated temperature rising caused by this pressure difference is estimated as small as 0.37 K.

The maximum and average temperature difference between wall and saturated refrigerant are 7.6 K and 3.9 K respectively except in the region of dry patch and dry out. From the results of heat transfer experiments and the flow observation, it is inferred that the convective evaporation is dominant and the nucleate boiling is fully suppressed.

Flow Pattern

Figure 5 shows the result of the flow observation with a high-speed camera and a digital still camera through a 30 mm thick transparent vinyl chloride resin plate placed as the front wall of the channel in order to observe the flow pattern during the evaporation process directory. Figures. (a)(stereogram), (b) (projected plane), (c)(projected plane) are the flow patterns of liquid film accompanied with dry patch, dripping and mist,

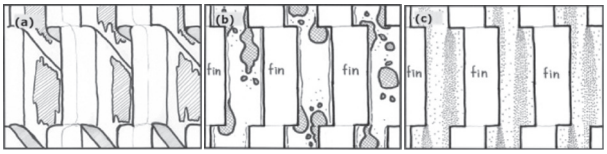

Fig. 5. Flow patterns
(a) Liquid film accompanied with dry patch
(b) Liquid film accompanied with dripping
(c) Liquid film accompanied with mist

respectively, where the shaded part in Figure(a) denotes dry part of the heat transfer area, the hatched part in Figure(b) denotes liquid drop or liquid film thicker than other parts and a dot in Figure(c) denotes a mist particle.

In the case of small G, despite the magnitude of q, the dry patch appears on the middle part of fin surface, as shown in Figure(a). The reason of dry patch is that the liquid gathers at larger curvature parts (top and root) of the fin and its flow rate is not sufficient for wetting the whole fin surface. The area of dry patch enlarges in the downstream region. Therefore, heat transfer coefficient α decreases with increase of quality x. This phenomenon is observed more clearly when q increases. In the case of large G, the dry patch does not appear in the whole region from upstream to downstream. In the upstream region liquid flows down mainly on the root and the top parts of fins and is not entrained to the gas phase. In the middle- stream region, drip from the trailing edge of a fin to the leading edge of a fin after next, as shown in Figure(b). α starts to increase with increase in x. The reason of the dripping is that the shear stress acting on liquid-vapor interface becomes larger due to the increase of the vapor velocity. In the downstream region, as shown in Figure(c), the liquid dripping turns into spraying, and the mist generation is much enhanced as the vapor velocity increases. The value of α rise much more with increasing of x. Most of the generated mist collide with the leading edge of the fin after next and make a thin liquid film on the fin surface again. This flow pattern is the mist flow type with the thin liquid film on the fin surface.

It is confirmed that the disturbance of liquid film is small in the whole region from upstream to downstream in the case of small G, while in the case of large G, that becomes violently with increase of q. It is also noted that nucleate boiling is not observed through the present experiments. In addition, flow pattern map was indicated in Ohara, J. and Koyama, S., (2012)

Characteristics of Heat Transfer

Figure 6(a), (b), (c) and (d) show the relation between heat transfer coefficient α and quality x in the case of q= 20, 30, 40 and 50 kW/m^2, respectively, where symbols of triangle, square, inverted triangle and circle represent the data of G= 28, 40, 55 and 70 kg/(m^{2}s), respectively. In each figure, in the case of G= 55, 70 kW/(m^{2}s), the value of α firstly decreases and then increases with increase of x. The main reason for the increase of α is considered that the flow pattern becomes dripping (Figure 5(b)) in the middle-stream region, and turns into mist flow with thin liquid film on the fin surface in the downstream region (Figure 5(c)). On the other hand, in the case of G= 28 kg/(m^{2}s), the value of α decreases in some degree with increase of x. This fact is seen from figures (a), (b), (c) and (d) that the value of α in the range $x \leq 0.3$ is almost independent of the magnitude of q and G, being almost constant about 9.5 kW/(m^{2}K). When the liquid film is laminar, the value of α is supposed to decreases with the increase of G (in other words, increase of film thickness). In these results, however, α does not decrease with the increase of G. It can be inferred from this fact that the disturbance of liquid film is promoted with the increase of G. Comparing α at constant values of G and x in these figures, it is seen that α decrease with the increase of q.

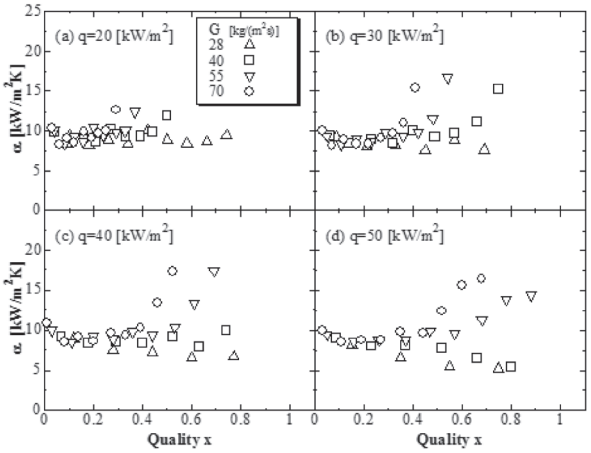

Fig. 6. The relation between α and x

Figure 7(a), (b), (c) and (d) show the relation between α/α_{lo} and $1/X_{tt}$ in the case of G= 28, 40, 55, and 70 kg/(m^{2}s), respectively, where X_{tt} is the Lockhart-Maltinelli' s parameter defined as

$$X_{tt} = \left(\frac{1-x}{x}\right)^{0.9}\left(\frac{\rho_v}{\rho_l}\right)^{0.5}\left(\frac{\mu_l}{\mu_v}\right)^{0.1} \qquad (6)$$

and α_{lo} is the heat transfer coefficient supposed that the liquid component only flows in the passage of heat exchanger, defined

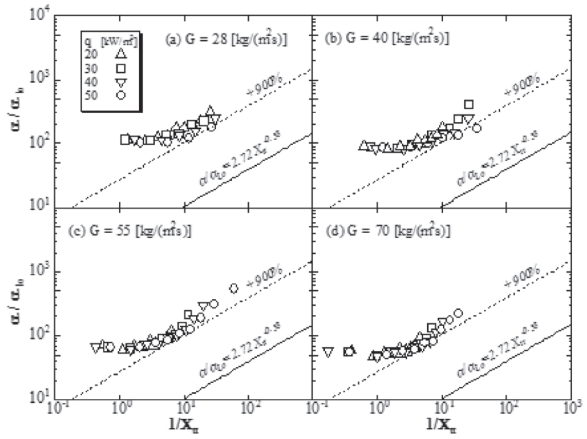

Fig. 7. The relation between α/α_{lo} and $1/X_{tt}$

as

$$\alpha_{lo} = 0.023 \frac{\lambda}{d_h} Re_l^{0.8} Pr_l^{0.4} \quad (7)$$

where d_h is a hydraulic diameter and the Reynolds number Re_l is defined as

$$Re_l = G(1-x)d_h/\mu_l \quad (8)$$

symbols of triangle, square, inverted triangle and circle represent the case of q= 20, 30, 40 and 50kW/m$_2$, respectively. The solid line is the heat transfer correlation equation for downflow forced convective evaporation in a vertical tube proposed by Wright[12].

$$\frac{\alpha}{\alpha_{lo}} = 2.72\left(\frac{1}{X_{tt}}\right)^{0.85} \quad (9)$$

In each figure, in the region of small $1/X_{tt}$ the value of α/α_{lo} keeps constant, while in the other range it increases with the increase of $1/X_{tt}$. It is also found from these figures that there is little effect of q and G on the relation between α/α_{lo} and $1/X_{tt}$. The data in the region of large $1/X_{tt}$ is ten times the value given by Wright' s correlation equation.

Heat Transfer Correlation Equations

Figure 8 shows the relation between Nusselt number Nu and two phase Reynolds number Re_{lv}, where Nu and Re_{lv} are defined as

$$Nu = \frac{\alpha d_h}{\lambda} \quad (10)$$

$$Re_{lv} = \frac{G_x}{\rho_v}\frac{d_h}{v_l} \quad (11)$$

In the figure, symbol colors of blue, green, orange and red represent the data of G= 28, 40, 55 and 70 kg/(m^{2}s), respectively. And shapes of symbols; inverted triangle, square, triangle and circle represent the data of q= 20, 30, 40 and 50 kW/m^2, respectively. The value of Nu is almost constant

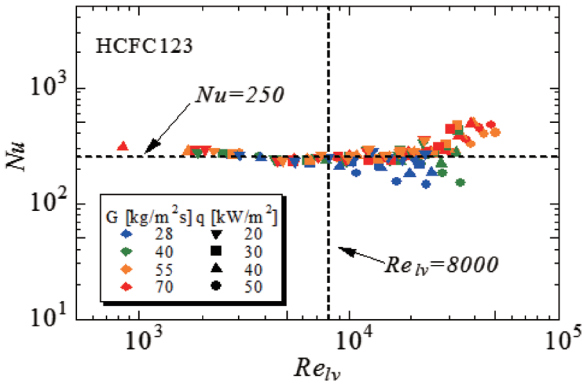

Fig. 8. Relation between Nu and Re_{lv}

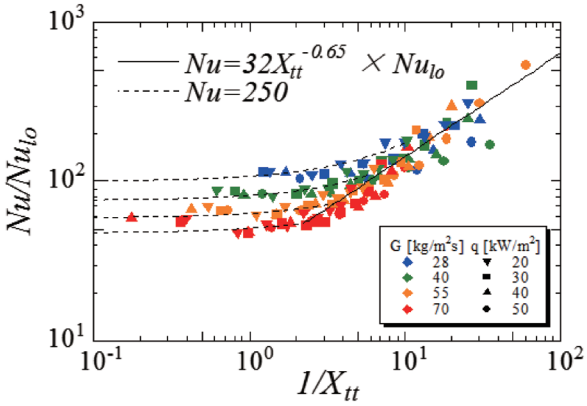

independently of q and G when $Re_{lv} \leq 8000$. In the region of $Re_{lv} \geq 8000$, Nu increases with increasing of Re_{lv}. Based on the above results, empirical correlation equations for heat transfer coefficient in a vertical falling film plate-fin evaporator are proposed as equations

$$Nu = \begin{cases} 250 \\ 32X_{tt}^{-0.65}Nu_{lo} \end{cases} \quad (12)$$

where, Nu_{lo} is Nusselt number of single phase turbulent flow based on the equation of Dittus-Bŏelter, and is defined as following equation.

$$Nu_{lo} = 0.023 Re_l^{0.8} Pr_l^{0.4} \quad (13)$$

Using equations (12), a greater value of Nusselt number should be chosen.

Figure 9 shows a relation between Nu/Nu_{lo} and $1/X_{tt}$. Symbols and lines represent the experimental data and the calculated result using equation (12) respectively. The data excepted for dry out region are well correlated within error of ± 30%. In this research, a boundary between equations (12) is that the value of two phase Reynolds number $Re_{lv} \cong 8000 \sim 15000$.

Fin Efficiency

Figure10 shows a physical model to evaluate the heat transfer

coefficient of the minichannel surface with fins. In this model, the following assumptions are employed: (1) the heat conduction in a fin is one dimensional along the fin surface, and (2) the heat transfer coefficient is constant in both of the fin and base surfaces. Based on this model, the local heat transfer coefficient α_{fi} is defined as

$$\alpha_{fi} \equiv \frac{Q_i}{\{A_i - A_{fi}(1-\eta_i)\}(T_{wi} - T_{sati})} \qquad (14)$$

where, A_i and A_{fi} are total heat transfer area of a section and fins respectively, T_{wi} and T_{sati} are the wall temperature and refrigerant saturation temperature of the i th section, respectively, and ηi is the efficiency of the i th section. The function of η_i is calculated as

$$\eta_i = \frac{s}{2_l} \cdot \tanh\left(\sqrt{\frac{\alpha_{fi} s}{\lambda_f F}} b'\right) \Big/ \sqrt{\frac{\alpha_{fi} s}{\lambda_f F}} b' \qquad (15)$$

where, s is the circumferential length of the fin, F is the cross-sectional area of a fin and λ_f is the thermal conductivity of fins.

Figure 11 shows the relation between heat transfer coefficient taking into fin efficiency account α_{fi} and quality x. In the figure, colors of symbols and shapes of symbols represent the values of mass velocity G and heat flux q respectively. Distributive characteristic of heat transfer coefficient α_{fi} is as same as the case of heat transfer coefficient α evaluated from base heat transfer area qualitatively (see Figure 6). The distribution range of value of heat transfer coefficient α_{fi} is from 7.5 to 3.2 kW/m^{2}K.

Fig. 9. Relation between Nu/Nu_{lv} and $1/X_{tt}$

Figure 12 shows the value of fin efficiency η along the quality x. The average value of η is about 0.6. In the region of $x \leq 0.3$, η is almost independent of the magnitude of q and G, being almost constant. While in the region of $x \geq 0.3$, data disperse widely from 0.42 to 0.76. Data of fin efficiency seems having inverse distributive characteristic of heat transfer coefficient in the Figure 11. It could be understand from equations (14) and (15).

CONCLUSIONS

Heat transfer characteristics and flow patterns are investigated experimentally for vertical falling film evaporation of pure refrigerant HCFC123 in rectangular minichannels consisting of offset strip fins. The following major conclusions are derived from this study:

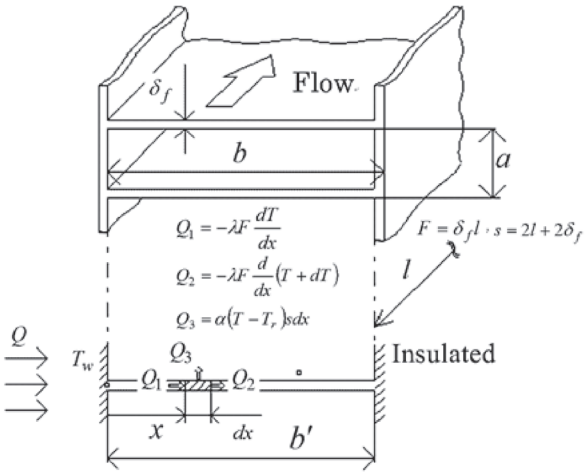

Fig. 10. Physical model of fin

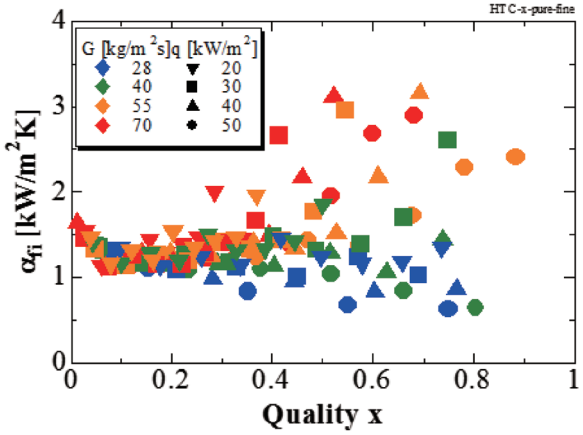

Fig. 11. The relation between α and x

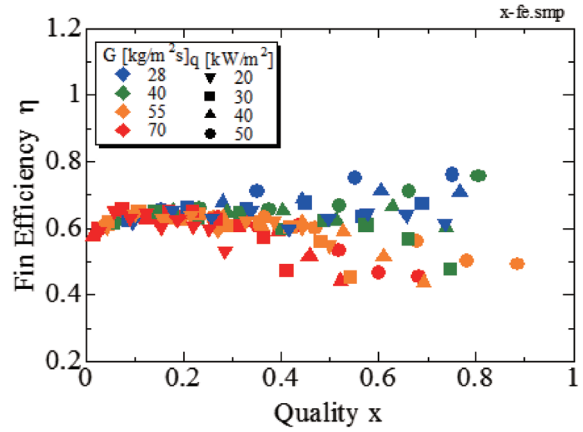

Fig. 12. The value of Fin efficiency

(1) From the direct observation, the flow pattern is classified into five typical types: plane liquid film, wavy liquid film, liquid film accompanied with dry patch, liquid film accompanied with dripping and liquid film accompanied with mist.

(2) In the case of small mass velocity G= 28 kg/(m^{2}s) and heat flux q= 20~50 kW/m^2, dry patch appears on the middle part of each fin surface in the upstream region (low quality region). As evaporation proceeds further, the area of each dry patch becomes

larger, and the heat transfer coefficient α decreases gradually, and ranging from 5 to 9 kW/(m^{2}K) in this case.

(3) As G increases, dry patch is not observed, but the disturbance of liquid film is observed in the upstream region. In the middle-stream region, the liquid starts to drip, and the value of α starts to increase in the flow direction. In the downstream region, the liquid dripping turns into spraying, and the mist generation occurs. The flow pattern is the mist flow type with thin liquid film on fin surface. In this region, the value of α increases with increase of x, and ranges from 10 to 16 kW/(m^{2}K).

(4) The experimental data of heat transfer coefficient are compared with Wright's equation for forced convective evaporation. The data agree with about ten times of Wright's equation in the region of large $1/X_{tt}$. In the region of small $1/X_{tt}$ the value of α/α_{lo} keeps constant.

(5) Heat transfer correlation equation for vertical falling film plate fin evaporator is proposed as

$$Nu = \begin{cases} 250 \\ 32X_{tt}^{-0.65}Nu_{lo} \end{cases}$$

This equation agrees with the experimental data within 30% deviation.

(6) From the results of fin efficiency analysis, distributive characteristic of heat transfer coefficient taking into account fin efficiency α_{fi} is as same as the case of heat transfer coefficient α evaluated from base heat transfer area qualitatively. The value takes from 7.5 to 3.2 kW/m^{2}K, and the average value of fin efficiency becomes about 0.6. The data of fin efficiency seems having inverse distributive characteristic of heat transfer coefficient.

REFERENCES

1) Rovertson, J. M., and Lovegrove, P. C.: Boiling heat transfer with freon 11 brazed-aluminum plate fin heat exchanger. Trans. ASME J of Heat Transfer, **105**, 605-610 (1983)

2) Thome, J. R.: Enhanced boiling heat transfer. New York Hemisphere Publishing Corporation, 323-351 (1990)

3) Kanlikar, S. G.: A model correlating flow boiling heat transfer in augmented tubes and compact evaporators", Trans. ASME, **113**, 966-972 (1991)

4) Feldmana A., Marvilletb C., Lebouche M.: Nucleate and convective boiling in plate-fin heat exchangers, Int Jo of Heat and Mass Transfer, **43**, 3433-3442. (2000)

5) Watel B.: Review of saturated flow boiling in small passages of compact heat-exchangers. Int Jo of Thermal Sciences, **42**, 107-140 (2003)

6) Kim B., and Sohn B.: An experimental study of flow boiling in a rectangular channel with offset strip fins. Int J of Heat and Fluid Flow, **27,** 514-521 (2006)

7) Pulvirenti B., Matalone A. and Barucca U.: Boiling heat transfer in narrow channels with offset strip fins: Application to electronic chipsets cooling, Applied Thermal Engineering **30**, 2138-2145 (2010)

8) Ribatski G. and Jacobi A.M.: Falling-film evaporation on horizontal tubes-a critical review. Int J of Refrigeration, **28**, 635-653 (2005)

9) Yang L. and Shen S.: Experimental study of falling film evaporation heat transfer outside horizontal tubes. Desalination ,**220**, 654-660 (2008)

10) Cherif A.S. et al.: Intensification of the liquid film evaporation in a vertical channel. Desalination, **250**, 433-437 (2010)

11) Ohara, J. and Koyama, S.: Falling film evaporation of pure refrigerant HCFC123 in a plate-fin heat exchanger. J of Enhanced Heat Transfer, **19**, 301-311 (2012)

12) Wright, R. M.: Downflow forced convection boiling in uniformly heated tubes. USAEC Rep. UCRL, (1961).